The influence of the glymphatic system on α-synuclein propagation: the role of aquaporin-4

Douglas M. Lopes,[1] Sophie K. Llewellyn,[1] Sheila E. Bury,[1] Jiazheng Wang,[1] Jack A. Wells,[1], Matthew E. Gegg,[2] Guglielmo Verona,[3] Mark F. Lythgoe[1] and Ian F. Harrison[1]

Abstract

Propagation and aggregation of prion proteins, such as tau and α-synuclein (αSyn), are key pathological features of neurodegenerative diseases. Extracellular clearance pathways, such as the glymphatic system, may play a crucial role in the removal of these toxic proteins from the brain. Primarily active during sleep, this system relies on aquaporin-4 (AQP4) water channel expression and polarisation to astrocytic endfeet, facilitating interstitial solute clearance. Glymphatic dysfunction has recently been implicated in Parkinson's disease, however the precise mechanisms underlying the pathogenic effect of this dysfunction remain unclear. This includes how impaired glymphatic function influences αSyn propagation dynamics, and the role of propagating αSyn itself on glymphatic function.

In this study, we used a mouse model of αSyn propagation to elucidate the impact of αSyn aggregation on glymphatic function, by measuring CSF-ISF exchange and assessing AQP4 and associated endfoot complex proteins in the brain over time and across different regions. Our results show that direct injection of αSyn pre-formed fibrils leads to local reduced expression of the AQP4 endfoot complex, but propagation of αSyn pathology induces an enhancement of glymphatic function suggesting compensatory upregulation in response to increasing αSyn aggregate load. To determine the influence of glymphatic dysfunction on αSyn propagation dynamics, we then employed a pharmacological approach to inhibit glymphatic function in this model. Acute glymphatic inhibition significantly reduced brain to CSF clearance of misfolded αSyn, and chronic treatment exacerbated αSyn pathology, cerebral atrophy, and motor behavioural deficits in mice. Together our findings show that αSyn clearance and propagation are modulated by glymphatic function. Moreover, they suggest that AQP4 complex dysregulation may contribute to glymphatic

impairment associated with Parkinson's diseases, supporting further mechanistic investigation of this protein complex in the disease.

Author affiliations:

1 Centre for Advanced Biomedical Imaging, Department of Imaging, Division of Medicine, University College London, London, WC1E 6DD, UK

2 Department of Clinical and Movement Neuroscience, UCL Queen Square Institute of Neurology, London, WC1N 3BG, UK

3 Centre for Amyloidosis and Acute Phase Proteins, Department of Inflammation, Division of Medicine, University College London, London, NW3 2PF, UK

Correspondence to: Ian F Harison

Centre for Advanced Biomedical Imaging, Paul O'Gorman Building, 72 Huntley Street, London, WC1E 6DD, UK

E-mail: ian.harrison@ucl.ac.uk

Running title: Aquaporin-4 and α-synuclein propagation

Keywords: glymphatic; alpha-synuclein; Parkinson's; propagation; aquaporin-4

Introduction

The accumulation of misfolded amyloid-structured 'prion-like' proteins is a pathological hallmark of neurodegenerative disorders such as Alzheimer's disease, Parkinson's disease, and Huntington's disease.[1] As with other 'prion-like' proteins, the phenomenon of α-synuclein (αSyn) propagation in synucleinopathies is thought to be achieved by the initial release of an αSyn 'seed' into the extracellular space, transportation/transference into other cells, templating of intracellular fibrillar structures of αSyn and initiation of a self-amplifying cascade of accumulation, leading to

further release of αSyn 'seeds'.[2-4] Evidence is therefore mounting to suggest that extracellular clearance pathways might represent therapeutic potential for management of these toxic proteins, limiting their propagation throughout the brain.[2,4] The glymphatic system is one such pathway, involved in clearance of metabolic waste products from the extracellular space in the central nervous system, which may represent a powerful determinant of propagation and progression of αSyn pathology in the brain.[5] Predominantly active during sleep,[6] this system is modelled on the inflow of cerebrospinal fluid (CSF) along perivascular spaces surrounding cerebral arteries, which then disperses throughout the brain interstitium via exchange with interstitial fluid (ISF), resulting in efflux of fluid and extracellular solutes via veinous perivascular space drainage out of the brain.[5,7] Most compelling, lack of sleep is rapidly becoming recognised as a pathological driver of protein aggregation in neurodegenerative disease,[8,9] and sleep may act to enhance protein clearance from brain,[7,10] providing rationale for study of the function of this system in relation to clearance of 'prion-like' proteins from the brain.[2]

Glymphatic perivascular fluid transport relies on the water channel aquaporin-4 (AQP4), which is predominantly expressed on the astrocytic endfeet that ensheathe cerebral vasculature.[11,12] AQP4 deletion thus causes significantly suppressed CSF-ISF exchange and reduced clearance of β-amyloid,[13,14] tau[15-17] and αSyn[18,19] from the brain. Not only is AQP4 expression essential, but its appropriate polarisation to astrocytic endfeet is required for efficient glymphatic and solute clearance.[12,16,20-22] Like the function of the glymphatic system, organisation of AQP4 in this way declines with age,[23,24] suggesting that impaired glymphatic function may contribute to the vulnerability of the aged brain to aberrant protein deposition, and as such, the onset of sporadic neurodegenerative disease. There is a growing body of evidence to suggest impaired glymphatic function in α-synucleinopathies such as Parkinson's disease,[25-31] but the causes of this are as yet unknown.

In this study, we make use of a mouse model of αSyn propagation, to better understand the effects of propagating αSyn aggregation on glymphatic function. We first measure glymphatic function and examine expression levels of AQP4 and its endfoot protein complex binding partners, both temporally and spatially in the brain. We then use a pharmacological approach to inhibit glymphatic function in this model setting, to determine whether impaired glymphatic function can accelerate or exacerbate αSyn aggregation and neuropathology in the brain.

Materials and methods

Generation and validation of αSyn pre-formed fibrils

αSyn pre-formed fibrils (PFFs) were formed from recombinant human wildtype αSyn as previously described.[32] Once formulated, PFFs were extensively validated ahead of their *in vivo* use. See supplementary materials and methods for full details of PFF generation and validation experiments.

Animals

Tg(Prnp-SNCA*A53T)83Vle were generated by Prof Virginia Lee[33] and were obtained from Jackson Laboratories (stock no.: 004479). Mice were hemizygously bred and homozygous offspring (henceforth referred to as M83 mice) were used for experiments at 2-5 months-of-age. Age-matched C75Bl6/J mice (henceforth referred to as wildtype mice) were used as controls and obtained from Charles River, UK. Animals were housed on a 12-hr light/dark cycle in groups of two to five in individually ventilated cages with *ad libitum* access to food and water and provided with environmental enrichment (cardboard houses and tubes, paper nesting). Equal numbers of both male and female animals were used in experimental groups, with required n numbers calculated *a priori* using appropriate power calculations and estimated effect sizes from the literature. 166 animals in total were used in this study. All animal work was performed in accordance with the UK's Animals (Scientific Procedures) Act of 1986 and approved by UCL's internal Animal Welfare and Ethical Review Board.

Intracerebral injection of αSyn

Mice (2 months-of-age) were anesthetized with 2% isoflurane in O_2 at a delivery rate of 1 l/min and positioned in a stereotaxic frame in the horizontal skull position. Buprenorphine (Vetergesic, 0.1 mg/kg, subcutaneously) was administered for peri/post-operative analgesia, prior to making a

midline incision on the top of the head to expose the skull. A burr hole was then made with a microdrill above the injection location (+0.2 mm anteroposterior, and +2 mm mediolateral to bregma). 2.5 µl/site of either sonicated αSyn PFFs or monomers (both at 2 mg/ml, 5 µg/site) were unilaterally infused at a rate of 0.5 µl/min into the striatum and overlying cortex (-1.8 and −0.8 mm ventrodorsal to the brain surface respectively) using a 5 µl Hamilton syringe. After each infusion, the needle was left *in situ* for 5 min to prevent injectate reflux. The scalp was then sutured closed, and the animal left to recover in a heated recovery chamber until it had regained consciousness. It was then returned to its home cage, and its weight monitored daily for 7 days post-surgery to ensure complete recovery.

mRNA and protein extraction and analysis

For time course expression studies, mice received intrastriatal/cortical injections with αSyn PFFs or monomers as above, and were left to age for the appropriate time period, after which animals were killed by overdose of sodium pentoparbital (10 ml/kg, intraperitoneally (i.p.)), the brain was removed from the skull and the ipsilateral and contralateral striatal and midbrain tissue was rapidly dissected out. Excised tissue was snap frozen immediately on dry ice and stored at -80 °C until further processing. mRNA in excised brain samples was extracted for quantification of AQP4 and dystrophin-associated complex (DAC) element expression, and corresponding protein extracts were used for Western blot quantification of αSyn (see supplementary materials and methods for full details).

Cisterna magna infusion for assessment of glymphatic function

Glymphatic function was assessed in the mouse brain by infusion of a fluorescent tracer to the cisterna magna, followed by brain slice imaging for quantification of CSF-brain influx, similar to that previously published by our group.[34] Briefly, mice received a cisterna magna infusion of low molecular weight fluorescent tracer, fixable Texas Red™-conjugated dextran (TxR-d3, 3 kDa; ThermoFisher) at 0.05% in filtered artificial CSF (Tocris). 10 µl of the tracer was infused at

2 µl/min over 5 min. 30 mins after the start of the infusion, animals were culled, and brains removed for sectioning and imaging. See supplementary materials and methods for full details.

Drug treatments

Glymphatic inhibition was achieved using TGN-020 (N-1,3,4- thiadiazol-2-yl-3-pyridinecarboxamide, Tocris Bioscience). Mice were treated i.p. with either TGN-020 (50 mg/kg in 20 ml/kg 0.9% sodium chloride (saline)) or vehicle (20 ml/kg saline). For acute studies, animals were randomly assigned to treatment groups and were given a single i.p. injection of either TGN-020 or vehicle. For chronic studies, animals were randomly assigned to treatment groups and were given i.p. injections of either TGN-020 or vehicle three times per week for 6 weeks (alternating the injection side each day and injecting animals in a random order), starting ~3 days post-surgery.

Assessment of acute αSyn clearance

Following acute treatment with TGN-020, αSyn PFFs were injected unilaterally into the striatum as described above (5 µg delivered in 2 mg/ml at 0.5 µl/min, +0.2 mm anteroposterior and +2 mm mediolateral to bregma and -1.8 mm ventrodorsal to the brain surface). The needle was left *in situ* while the cisterna magna was surgically exposed (also described above) and cleaned with an ethanol soaked swab. 15 min after the start of the striatal injection a durotomy was performed using a 23-gauge needle, allowing free-flowing CSF to be collected using a narrow bore pipette tip. Following collection, mice were killed by overdose with sodium pentobarbital (10 ml/kg, i.p.). The brain was removed from the skull and snap frozen immediately on dry ice and stored at -80 °C until further processing. The collected CSF was centrifuged briefly to pellet any red blood cell contamination. Hypotonically disrupted blood cell contaminants (freeze-thawing of rehydrated blood pellets) were spectrophotometrically analysed (417 nm, NanoDrop ND-1000, Fisher Scientific), and samples found to contain >1% blood contamination were excluded from downstream analysis (one sample from the acute clearance study, three samples (one from each treatment group) from the chronic treatment study). Contamination was measured to be <0.01% in all remaining samples. Total tau concentration in CSF samples and homogenised (10% (w/v) in

sterile PBS containing protease inhibitor cocktail, phosphatase inhibitor cocktails I and II (Sigma), at a final dilution of 1:100, and 1 mM phenylmethylsulphonyl fluoride) brain tissue was quantified by dot blot (described above) using a conformation-specific anti-αSyn antibody ([MJFR-14-6-4-2], Abcam), and diluted PFFs as a standard series. The total mass of αSyn left in the brain and the concentration of PFFs in extracted CSF were calculated.

Open field task

The open field task was used to test for motor impairments. The apparatus consisted of a 45 × 45 × 45 cm white Perspex box open at the top. At the start of the test the mouse was placed in the centre of the field, and allowed to explore the apparatus for 5 min. The open field was thoroughly cleaned with 70% ethanol in between trials. Each mouse was recorded using a digital video camera (Konig, CASC300) placed approximately 50 cm above the apparatus. Animals' paths were tracked using AnimalTracker (http://animaltracker.elte.hu/), which automatically determined the distance travelled and time spent in the central and peripheral areas of the field. Path tracking analysis was carried out with the experimenter blind to experimental/treatment group.

Magnetic resonance imaging

At the end of drug treatment studies (6 weeks post-αSyn injection), structural 3D MR images of mouse brains were acquired. For this, mice were anesthetized with 2% isoflurane in a mixture of air (0.4 l/min) and O_2 (0.1 l/min), and positioned into an MR-compatible stereotaxic frame, with 1.5% isoflurane delivered (in the same gas mixture) via a nose cone. A horizontal-bore 9.4T Bruker preclinical system (BioSpec 94/20 USR, Bruker) was used for acquisition of isotropic 3D structural T_2-weighted MR images of the entirety of the mouse brain, using a volume coil and 4-channel surface coil for radiofrequency transmission and signal detection, respectively. A fast spin echo sequence with the following parameters was used: FOV = 16 × 16 × 16 mm, matrix = 128 × 128 × 128, repetition time = 700 ms, echo time = 40 ms, 2 averages.

For analysis, ITK-SNAP (v4.2.0)[35] was used for manual segmentation of the striatum, midbrain, cortex and hippocampus, referring to the Allen Mouse Brain Reference Atlas (https://mouse.brain-map.org/static/atlas) for anatomical guidance. Segmentation was performed (blind to animal treatment group) primarily in the coronal plane, with adjustment of regions-of-interest (ROIs) boundaries in the other two imaging planes. ROI pixel numbers were converted to volumes which are presented by multiplying by the pixel volume (0.001953125 mm^3). Two animal scans were excluded to due image motion artefacts precluding accurate segmentation.

Immunohistochemistry

At the end of chronic treatment experiments, CSF samples were extracted from the cisterna magna for quantification of αSyn content (as described above) prior to perfuse fixation of mice. For this, mice were injected with an overdose of sodium pentobarbital (10 ml/kg, i.p.) and transcardially perfused with approximately 10 ml PBS immediately followed by the same volume of 4% PFA. Brains were extracted from the skull and drop-fixed in 4% PFA for 24 hrs at 4 °C. Brains were then cryopreserved (30% sucrose in PBS for 72 h at 4 °C), freeze embedded in OCT, and serial coronal sections collected (50 µm thick) onto SuperFrost Plus™ microscope slides (VWR) using a cryostat (CM3050 S, Leica). Slides were stored at -20 °C until further processing.

Sections were stained using a conformation-specific anti-αSyn antibody ([MJFR-14-6-4-2], Abcam, see supplementary materials and methods for full details) and single plane, tiled images were captured on a fluorescence microscope (Leica DMi8) using a 10 × 1.3 NA objective. For analysis, using ImageJ (v1.51j8), a ROI was drawn on images encompassing the striatum in at least 6 sections from each brain, with the experimenter blind to animal experimental/treatment group. Measures of % area coverage (after thresholding for immunoreactivity) were extracted from each and averaged across slides analysed from each brain.

Statistical analysis

All data is presented as group means ± standard error of the mean (SEM), with individual datapoints shown where possible. For comparisons between groups, either 1-way or 2-way Analysis of Variance (ANOVA) was used, depending on the dataset (ANOVA type denoted on individual graphs), with either Tukey's multiple comparisons tests for individual comparisons, or Šidák's or Bonferroni multiple comparisons tests for grouped data comparisons. For XY plots, simple linear regression analyses were used to test for correlations. For the kinetic ThT assay, data was fitted to a sigmoidal four parameter curve, extracting 50% maximal ($Time_{50}$) values. All graphs were constructed, and statistical comparisons made using GraphPad Prism (v10.3.0).

Results

αSyn PFFs exhibit amyloid characteristics and induce propagation *in vitro* and *in vivo*

Amyloid αSyn PFFs were generated from recombinant human wildtype αSyn by agitation,[32,36] for subsequent injection and induction of pathological αSyn propagation *in vivo*. Successful conversion of monomers to fibrils was first confirmed by sedimentation. Following centrifugation, significantly greater protein was observed in the pellet compared to supernatant fractions of PFF samples ($p<0.0001$), and the inverse was seen in the monomeric starting material ($p<0.0001$) (**Fig. 1A, B**), indicating successful conversion to fibrils. The presence of amyloid structures was then confirmed by ThT fluorescence. Significantly greater fluorescence was observed when ThT was incubated with PFFs compared to monomers and all other controls ($p<0.01$ in all comparisons) (**Fig. 1C**). To confirm the presence of αSyn aggregates, dot blot analysis was utilised, with an antibody against conformation-specific αSyn ([MJFR-14-6-4-2], Abcam) (**Fig. 1D**). Increasing immunoreactivity with loaded protein was seen in both sonicated and unsonicated PFFs samples, but not with monomers (**Fig. 1D, E**). The ability of the generated PFFs to seed aggregation was then assessed, by agitation of αSyn monomers with PFF samples (1:100 PFF to monomer ratio) in the presence of ThT. Both sonicated and unsonicated PFFs significantly reduced the aggregation

time of monomeric αSyn (p<0.0001 in both comparisons, inset, **Fig. 1F**), but sonicated PFF reduced this time further, by 4.89 hrs (**Fig. 1F),** indicating significant seeding capacity.

In order to confirm the seeding capacity of PFFs *in vitro* ahead of injection, SH-SY5Y cells overexpressing αSyn with a hemagglutinin (HA) tag[37] were treated with monomeric αSyn, unsonicated or sonicated PFFs. Treatment with sonicated PFFs increased the level of TX-100 insoluble (solubilized with urea-SDS) αSyn phosphorylated at Ser129 (**Fig. 1G**). Sonicated PFFs also increased the level of HA-αSyn, indicating propagated accumulation of endogenously expressed αSyn in cells (**Fig. 1G**), and induced higher molecular weight (HMW) insoluble αSyn species (**Fig. 1G**), indicating PFF-induced αSyn aggregation.

Lastly to confirm seeding capacity and the ability of generated PFFs to induce propagation of αSyn pathology i*n vivo*, homozygous M83 mice (2 months-of-age) were injected with either monomers or sonicated PFFs into the left striatum and overlying cortex, as previously described,[36] and left to age for 6 weeks. Immunofluorescence staining for αSyn aggregation ([MJFR-14-6-4-2], Abcam), revealed substantial intracellular αSyn accumulations (**Fig. 1H**, arrowheads) and αSyn-positive neurite processes (**Fig. 1H**, arrows) in both the ipsilateral and contralateral striatum of PFF injected mice, but not in monomer injected animals. Together, these data indicate successful generation of αSyn PFFs from recombinant human wildtype protein, capable of pathological propagation induction *in vivo*.

αSyn PFF seeding causes dystrophin associated complex dysregulation *in vivo*

For study of glymphatic mechanisms, cohorts of homozygous M83 mice (2 months-of-age) were injected with either monomers or sonicated PFFs into the left striatum and overlying cortex to initiate αSyn propagation *in vivo*, as above and as previously described.[36] Seeding with PFFs in this way resulted in significant decline of striatal AQP4 and expression of elements of the AQP4 DAC compared to monomer injected controls, as early as 2 weeks post-injection (58.7% expression reduction on average in PFF injected mice compared to wildtype baseline, vs. 14.0% expression increase on average in monomer injected mice at the same timepoint, p<0.0001, **Fig.**

2A, B, C). This decline in AQP4 and DAC element expression in PFF injected mice continued to develop with time (66.6% and 76.3% expression reductions on average at weeks 4 and 6 post-injection, respectively, $p<0.0001$ compared to monomer injected controls at both timepoints, **Fig. 2A, B, C**). Most interestingly, when DAC mRNA expression profiles were correlated to phosphorylated (at Ser129) αSyn protein load, negative associations were observed; reduced DAC element expression with increased αSyn load. The strength of these correlations reached significance in elements of the DAC most proximal to the water channel (**Fig. 2B**) (AQP4, $p=0.0294$, and SNTA1, $p=0.01$, **Fig. 2D**) and approached significance in the distal elements (DTNA, $p=0.0533$, DMD, $p=0.0805$, and DAG1, $p=0.0598$, **Fig. 2D**), suggesting that αSyn deposition and AQP4 complex integrity are in some way linked.

This was not the case in the midbrain however; no noticeable correlations were observed between DAC mRNA expression and αSyn load (all linear regression R_2 values <0.04, all p values >0.15, **Supplementary Fig. 1A**). This perhaps is not surprising, given that this rostral region of the brain receives αSyn only towards the later stages of pathological development in this model.[36] Consistently, at week 6 post-injection, reduced AQP4 complex expression was observed in the midbrain of PFF injected mice (29.6% expression reduction on average in PFF injected mice compared to wildtype baseline levels, $p<0.0001$ compared to transgenic baseline expression, **Supplementary Fig. 1B, C, D**), suggesting that propagated αSyn deposition may directly affect AQP4 complex integrity, despite no overall correlation existing in this brain region.

αSyn arrival coincides with glymphatic upregulation in the midbrain of PFF seeded mice

To investigate this suggestion further, we then assessed glymphatic function in this animal model. To our surprise, at weeks 4 and 6 post-injection, we observed enhanced bilateral tracer uptake in the midbrain of PFF injected mice following cisterna magna infusion, indicative of increased CSF-ISF exchange ($p=0.0020$ and $p=0.0062$ compared to transgenic baseline at weeks 4 and 6 respectively, **Fig. 3A, B**). This upregulation in PFF injected mice was significantly increased compared to monomer injected controls only at week 4 ($p=0.0403$), but not at week 6 ($p=0.4615$) however (**Fig. 3A, B**). Quantification of αSyn deposition in this same brain region revealed that

this glymphatic upregulation coincides with a surge in αSyn accumulation (p=0.0353 compared to respective timepoint levels in monomer injected controls, **Fig. 3C, D**), suggesting that perhaps glymphatic function is upregulated in response to the arrival of propagated αSyn at this timepoint. In contrast, no corresponding change in tracer uptake was observed in the striatum of PFF injected animals, despite direct injection of αSyn in this region (**Supplementary Fig. 2**). Glymphatic upregulation compared to transgenic baseline in the midbrain however persists to week 6 (p<0.01 compared to transgenic baseline levels, **Fig. 3A, B**), resulting in normalisation of deposited αSyn (**Fig. 3C, D**), despite downregulation of AQP4 and DAC element expression in this region at this timepoint (**Supp. Fig. 1A, B**).

Acute TGN-020 treatment reduces brain to CSF αSyn clearance

To investigate the relationship between glymphatic function and αSyn further, a pharmacological approach was taken for glymphatic inhibition; experimentally altering glymphatic function to determine the resultant effects on αSyn clearance from the brain. We have previously shown that acute TGN-020 treatment causes marked inhibition of glymphatic function.[15] Here, mice were systemically treated with either TGN-020 or vehicle prior to intrastriatal injection of either PFFs or aCSF. 15 min later, brain and CSF (from the cisterna magna) were collected for quantification of αSyn content by dot blot (**Fig. 4A, B**). TGN-020 treatment resulted in significantly greater αSyn retention in the brain compared to vehicle treatment (p=0.0492, **Fig. 4C**). Correspondingly, in the same mice, significantly reduced CSF αSyn was seen in drug treated mice compared to that observed in vehicle treated animals (p=0.0358, **Fig. 4D**). Together, these changes are consistent with glymphatic mediated clearance of αSyn.

Chronic TGN-020 treatment exacerbates pathology in the PFF-M83 model of αSyn propagation

We have previously shown that chronic treatment with TGN-020 results in sustained glymphatic inhibition,[34] and saw above that acute glymphatic inhibition resulted in reduced clearance of αSyn

from the brain. Therefore in order to determine whether a change in glymphatic function could affect disease progression *in vivo* in a disease model setting, as above, M83 mice (2 months-of-age) were injected with either monomers or PFFs (**Fig. 5A**) to initiate αSyn propagation,[36] and subsequently treated chronically with either TGN-020 or vehicle (**Fig. 5B**). Motor behaviour of mice was assessed by open field at baseline (prior to intracerebral injection) and after 6 weeks of treatment, and structural MRI scans were acquired at the end of the experiments prior to brain and CSF collection for downstream analysis (**Fig. 5B**).

TGN-020 treatment induced a locomotor phenotype in PFF seeded M83 mice. Drug treated animals exhibited significantly reduced distance travelled in the open field arena at week 6 compared to their baseline assessment (p=0.0005, **Fig. 5C**). This reduced locomotion of TGN-020 treated mice resulted in a significant increase in the time spent immobile in the arena, compared to both their own baseline assessment (p=0.0003, **Fig. 5D**), and also the vehicle treated PFF seeded group at week 6 (p=0.0069, **Fig. 5D**). No such differences were observed in monomer injected animals, or in PFF injected vehicle treated mice (**Fig. 5C, D**). In order to confirm that the observed impaired motor function was specific to transgenic mice seeded with PFFs, and also not a more general effect of drug treatment, experiments were repeated in wildtype animals. No motor deficits were observed in monomer injected wildtype animals, or in either TGN-020 or vehicle treated PFF seeded wildtype animals (**Supplementary Fig. 3A, B**), suggesting that the effect was unique to PFF seeded M83 mice, in which substantial αSyn propagation and deposition is observed (**Fig. 1H**).

Structural, anatomical MRI scans of mouse brains were acquired following 6 weeks of drug/vehicle treatment. In both PFF injected groups, significant atrophy was observed in the ipsilateral striatum compared to contralateral hemispheric volumes (p=0.0012 and p=0.0001, respectively, **Fig. 6A**). This interhemispheric difference was greater in TGN-020 treated mice however (16.27% in TGN-020 treated, and 12.80% in vehicle treated groups), and significantly reduced striatal volumes were observed in TGN-020 treated PFF injected mice compared to monomer injected vehicle treated controls (**Fig. 6A**). In the midbrain, significantly reduced volumes were observed in TGN-020 treated PFF injected mice compared to both PFF injected (p=0.0072) and monomer injected (p<0.0001) control mice (**Fig. 6B**). And TGN-020 treated animals were the only group in which significant ipsilateral atrophy was observed compared to contralateral volumes (p=0.0164, **Fig. 6B**). Outside of the nigrostriatal axis, in the cortex,

significant atrophy was observed in both PFF injected groups compared monomer injected controls (**Supplementary Fig. 4A**). However in the interconnected hippocampus, significant atrophy compared to monomer controls was observed only in TGN-020 treated, and not vehicle treated, PFF injected mice, consistent with exacerbated pathological spread (**Supplementary Fig. 4B**).

Following MRI acquisition, CSF samples were taken and brains collected for histology. Significantly greater levels of aggregated αSyn were observed in the striatum of TGN-020 treated PFF injected mice compared to both vehicle treated PFF injected (p=0.0048) and monomer injected (p<0.0001) controls (**Fig. 6C, D**). Furthermore, in the ipsilateral striatum, significantly greater αSyn was seen in TGN-020 treated mice compared to both PFF injected (p=0.0499) and monomer injected (p<0.0001) vehicle treated animals (**Fig. 6C, D**). Exacerbated αSyn deposition in the ipsilateral striatum of drug treated mice also resulted in a significant interhemispheric difference in these animals (p=0.0492, **Fig. 6C, D**). αSyn pathology was also detected in both the cortex and hippocampus of PFF injected transgenic animals, consistent with MRI data (**Supplementary Fig. 4C**), but no αSyn pathology was observable in wildtype mice injected with monomers or PFFs, or in PFF injected wildtype animals subsequently treated with TGN-020 (**Supplementary Fig. 3C**). Similar to what was observed following acute TGN-020 treatment in PFF injected M83 mice (**Fig. 4**), exacerbated αSyn load in the brain as a result of chronic drug treatment was accompanied by decreased CSF αSyn content: 90.33% reduction in PFF injected vehicle treated mice compared to monomer injected controls, and a further reduction of 7.53% (97.87% overall) in TGN-020 treated PFF injected mice compared to the monomer injected group (**Fig. 6E**).

Discussion

In the current study we used a mouse model of αSyn propagation to investigate how impaired glymphatic function influences αSyn propagation dynamics in the brain and the effect of propagating αSyn itself on glymphatic function. We show that inducing αSyn pathology *in vivo*, by injection of αSyn PFFs into the striatum, leads to a robust reduced expression profile of the AQP4 endfoot protein complex, which negatively correlates to phosphorylated αSyn load. Conversely, propagation of αSyn to the midbrain with time inspires an enhancement of glymphatic

function, which appears to manage the influx of propagating αSyn and normalises protein burden. To directly examine the influence of the glymphatic system on αSyn propagation and deposition, we then used a pharmacological approach to inhibit glymphatic clearance. Acute glymphatic inhibition reduced clearance of αSyn from brain to CSF, and extended inhibition of glymphatic function in PFF seeded mice led to exacerbated striatal αSyn pathology, striatal and midbrain atrophy, and motor behavioural deficits. Together, our data show that αSyn clearance and propagation are regulated by glymphatic function and suggest that AQP4 complex dysregulation may contribute to glymphatic impairment associated with Parkinson's disease.

Recent years has seen a surge in research publications suggesting impaired glymphatic function in α-synucleinopathies such as Parkinson's disease.[25-31] This body of work largely uses diffusion tensor imaging (DTI) and the 'DTI along the perivascular space' (DTI-ALPS) index as a non-invasive marker of glymphatic function, by isolating and measuring water diffusivity within perivascular spaces running parallel to deep medullary veins. The validity of DTI-ALPS as a marker for glymphatic function has recently been called into question,[38] but given the wealth of studies now highlighting the potential involvement of the glymphatic system in this class of neurodegenerative disease, further work is justified to ascertain the precise mechanisms underlying the contribution of glymphatic dysfunction to disease progression in α-synucleinopathy.

The relationship between neurodegenerative disease pathology and perivascular AQP4 has been explored in Alzheimer's,[39] but the involvement of glymphatic clearance in α-synucleinopathies remains largely under researched. Hoshi and colleagues examined AQP4 expression in the temporal neocortex of patients with Parkinson's disease and found a negative correlation between αSyn pathology and AQP4 expression.[40] We saw a similar relationship in the current study, in the striatum of mice seeded with αSyn, extending the observation to DAC proteins. To our knowledge however, AQP4 polarisation is yet to be quantified in the Parkinson's disease brain. But consistent with what has been shown post-mortem, our data suggests that not only is AQP4 affected in pathology, but so too is the complex of proteins which anchors the water channel at the membrane, facilitating the glymphatic clearance of solutes, including αSyn, from the brain.

There has been more work looking at the relationship between glymphatic function and αSyn pathology in the mouse brain however. Cui and colleagues showed that when AQP4 expression was reduced (heterozygous AQP4 knockout mice), αSyn pathology, dopaminergic

neurodegeneration, and motor behavioural impairments induced by injection of αSyn PFFs were exacerbated.[18] This study was recently added to by Zhang and colleagues, who showed that AQP4 deletion (homozygous knockout) intensified αSyn pathology and motor impairments as a result of viral-vector delivered A53T-αSyn into the substantia nigra.[19] Both of these studies suggest a clear role of AQP4 in regulating αSyn accumulation in the brain but are limited by their use of genetic approaches to manipulate glymphatic function *in vivo*; reduced AQP4 expression from birth, present at the time of pathology induction. We show here that (pharmacological) glymphatic inhibition results in a ~75% greater retention of intracerebrally delivered agents. By taking such a genetic approach, it is therefore impossible to isolate the effects of AQP4 reduction on pathological development from its effects on enhanced pathological induction. In our study, glymphatic function was pharmacologically inhibited *after* model establishment; mice receiving TGN-020 treatment starting ~3 days post-injection with PFFs. Hence, we can infer that the exacerbated pathology we saw in mice was a result of enhanced propagation and pathological development of αSyn pathology in the brain, rather than increased seeding, substantiating the suggestion that αSyn propagation and accumulation are regulated by the glymphatic system.

For many years, functional studies of the glymphatic system in relation to neurodegenerative disease pathology were focussed almost exclusively on the clearance of β-amyloid from the brain,e.g. [13,14] perhaps due to the extracellular nature of β-amyloid plaque pathology. But more recently, studies now implicate failure of the system in the accumulation of a number of intracellular proteins prone to brain-wide propagation.[15-19,41,42] For example, we recently published findings on the effects of glymphatic inhibition on tau propagation in a seeded mouse model[34]; enhanced propagation and accumulation of tau in the brain following chronic treatment with TGN-020. In that study, at end-stage following chronic TGN-020 treatment, we saw near off identical levels of exacerbated tau pathology in the hippocampus, to that of αSyn pathology we see here in the striatum, despite different durations of animal studies, different propagation models, and different pathology inducing injectates. Indeed, tau and αSyn are very different proteins (~55-62 kDa and 14 kDa, respectively), but it appears that their glymphatic clearance profiles are remarkably similar. Disease-associated glymphatic dysfunction and lack of clearance discrimination between neurodegenerative disease associated proteins might explain the mixed or concomitant pathologies which are increasingly reported and characterised in the literature; thought by many to be the norm rather than the exception in late-onset neurodegenerative

disease.[43-46] Given the number of protein pathologies the glymphatic system has now been implicated in, studies aiming to hierarchically classify the glymphatic clearance of neurodegenerative disease proteins might provide much needed direction for the field, with the hope of translating potential glymphatic targeting therapies to the clinic.

Aside from the effects of glymphatic inhibition we saw on αSyn pathological development, we also observed regional differences in PFF-induced alterations of glymphatic function, in PFF seeded mice. Glymphatic function in the striatum, which was subject to direct injection of PFFs, was relatively unaffected, but exhibited substantial AQP4 and DAC protein downregulation. Glymphatic function in the midbrain on the other hand, appeared to be upregulated upon receipt of αSyn, with AQP4 expression alterations found only at end-stage in the model. By contrast, Zhang et al. saw reduced glymphatic tracer influx in the whole brain 4 weeks after AAV-A53T injection into the substantia nigra, and reduced AQP4 polarisation in both the striatum and substantia nigra.[19] Similarly, in aged A53T transgenic mice, Zou and colleagues also saw reduced glymphatic inflow in the midbrain, but interestingly also observed increased AQP4 expression, but reduced polarisation in this region.[47] Both of these studies use ketamine/xylazine anaesthesia for glymphatic measurements, whereas in our study we use isoflurane, which has been shown to supress glymphatic function[48,49] and could therefore potentially account for the discrepancy. The other major difference between both of these studies and ours however is the method by which αSyn pathology is induced in the brain. Both Zhang and colleagues, and Zou and colleagues use a genetic approach to drive protein aggregation (via AAV injection or transgenic expression, respectively). Whereas, here, we induced pathological accumulation and propagation of αSyn via PFF injection. Although we perform these experiments in A53T mice, pathological seeding is induced in young animals, where transgene driven αSyn deposition is yet to occur[33]; transgenic expression of pre-pathological aggregate-prone αSyn accelerating rather than initiating pathology in the brain. The discrepancy between our results and both of the aforementioned studies suggests that propagating αSyn, and genetically overexpressed mutant αSyn, have marked differences in terms of their effects on glymphatic function. For example, in the current study we saw that when αSyn pathology physiologically propagates to the midbrain, in contrast to when it is genetically overexpressed and already deposited there, the glymphatic system is able to respond and increase its function. This gives us some insight into what might occur in the Parkinson's disease brain as αSyn pathology propagates and the disease progressed through the Braak stages[50]; the glymphatic

system is plastic in its nature and is able to upregulate its function in response to receipt of aggregate-prone proteins (what we saw in the midbrain in our study). Once protein deposition is established however (like in the striatum in our study, and end-stage in the midbrain) and neurodegeneration is evident, AQP4 expression becomes affected. We can infer from our drug study that reduced AQP4 expression likely exacerbates αSyn pathology, but much is still left to learn about precisely how αSyn, particularly propagating αSyn, affects AQP4 expression and channel function. Understanding the mechanisms by which these two proteins affect one another may provide information as to much needed novel drug targets for potential disease alteration.

Glymphatic function has similarly found to be impaired in non-αSyn based mouse models of Parkinson's. For example Si and colleagues found glymphatic inflow and tracer clearance to be impaired when dopaminergic neurodegeneration was induced by 1-Methyl-4-phenyl-1,2,3,6-tetrahydropyridine (MPTP) in mice.[51] Interestingly, in this setting, reduced glymphatic function was only seen to be impaired in the midbrain and substantia nigra (the location of the dopaminergic cell bodies undergoing degeneration) but not in the striatum (location of the dopaminergic terminals projecting from the nigra), despite significant declines in tyrosine hydroxylase positive signal observed at both locations. Similarly, in LRRK2 (mutations of which are the most common genetic cause of Parkinson's, and are associated with high risk of sporadic Parkinson's disease development)[52] mutant (R1441G) mice, glymphatic function and AQP4 polarisation were observed to be reduced.[53] The authors of this study also show that LRRK2 itself interacts with AQP4 to phosphorylate it, which leads to reduced polarisation of the channel. These studies add further insight into the wealth of potential influences biological perturbations in the Parkinson's brain may have on the function of the glymphatic system and highlight that although αSyn accumulation plays a substantial role in disease development and progression, its aggregation is not the only factor which likely affects the capacity of the glymphatic system to rid the brain of interstitial waste solutes.

Sold as an AQP4 inhibitor, TGN-020 has now been shown by numerous independent groups to inhibit glymphatic function *in vivo*.[51,54-59] Indeed, our own group has shown that both acute and chronic treatment with the agent reduces interstitial inflow of CSF tracers (both fluorescent and gadolinium-based).[15,34] In xenopus oocytes, TGN-020 has been shown to be isoform specific for AQP4 compared to other aquaporins, with an IC_{50} of 3.1 μM.[60] However reports suggest difficulty reproducing these cell-based assays,[61] with lack of drug effect observed in primary astrocytes

expressing endogenous AQP4 or mammalian cell-lines overexpressing exogenous AQP4.[62] Indeed, published *in vivo* studies using TGN-020 fail to clarify its mechanism of action, hence careful interpretation of results is required. In our hands, like many groups, we see robust glymphatic inhibition with TGN-020 *in vivo,*[15,34] but this raises the suggestion as to what other targets TGN-020 is interacting with to affect glymphatic function. AQP4 has been central to studies of the glymphatic system since its discovery, but the clear effect we see here of this drug on αSyn propagation and accumulation underscores the need for more in-depth study of its mechanism of action, *in vivo*, which may lead to identification of additional targets able to influence glymphatic function.

In the current study we made use of a transgenic model of αSyn propagation, in which pathology was seeded in the brain with αSyn PFFs, and propagation of αSyn pathology is accelerated by the transgenic expression of A53T mutant human αSyn. First described in 2012,[36] this model provides a robust platform on which to study mechanisms associated with the propagation of human αSyn in the brain, within a feasible experimental period, as we have here. Achievement of the model is reliant upon generation of suitable αSyn PFF seeding material, which is highly dependent on buffer conditions, sonication efficiency, and storage, hence large batch-to-batch and lab-to-lab variability has been reported, leading to reproducibility issues.[32,63] To minimise these in our study, we made use of the Michael J. Fox Foundation for Parkinson's Research (MJFF) guidelines and best practices for generating PFFs,[32] ensuring their thorough validation ahead of *in vivo* work and use of a single PFF batch for all work presented. Although within our own study we saw highly reproducible development of αSyn pathology in the brain, we observed substantial discrepancies in terms of the time course of disease phenotype observed in animals injected with our PFFs compared to other groups. Injection of our generated PFFs (5 µg, unilaterally) into the striatum and overlying cortex of M83 mice led to a median survival time (time to reach humane endpoint) of 61 days (data not shown), which was highly uniform as previously noted by others.[36] Hence in the current study we chose to treat animals with the glymphatic inhibitor for 6 weeks (42 days), to allow us to assess the extent to which drug treatment exacerbated pathology in the brain. The period of survival post-PFF injection in our characterisation of the model, was far shorter than Luk and colleagues, who originally described the model. Researchers reported a median survival time of 101 days, despite use of an identical PFF dose, injection site and transgenic mouse line for investigations.[36] The authors of this work also struggled to quantify motor impairments in their

mice due to the rapidity of which mice develop symptoms at end stage. Indeed, in vehicle treated PFF seeded mice in our study, we were unable to detect a motor impairment with open field at 6 weeks; only observing apparent locomotor reduction in drug treated animals at this timepoint. We also conducted vertical cylinder testing and grip strength testing on our animals at baseline, and at weeks 2, 4 and 6 post-PFF injection, but also failed to detect any motor impairment using these tests in any of the groups (data not shown). Our findings are hence more in line with Earls et al., who saw clinical symptoms (unstable gait and hunched posture with extensive hind limb retraction) at 70 days post-injection prior to brain collection at the end of their study, with a number of mouse deaths observed prior to this timepoint with their treatment, which exacerbated pathology.[64] Authors of this study interestingly also observed increased limb clasping behaviour in PFF injected M83 mice from 5 weeks post-injection and onwards. The notable discrepancies between studies using this model highlights how important thorough validation of the PFF seeding material is, and shows that although robust in-lab, this model is exceptionally prone to between-lab variability, serving as a warning to researchers to establish this model with caution, and ensure thorough characterisation of it in their own hands before embarking on large experimental cohort studies.

In conclusion, we have shown here that in a mouse model of αSyn propagation, the expression profiles of AQP4 and its endfoot binding partners are affected by phosphorylated αSyn load. Incoming propagation of αSyn in the midbrain however encourages an enhancement of glymphatic function in response, to manage αSyn burden, ahead of AQP4 and endfoot protein dysregulation. Experimental inhibition of glymphatic function in mice reduces brain to CSF clearance of αSyn acutely and exaggerates pathology and behavioural impairments in an extended treatment paradigm. Together our findings suggest that αSyn-induced dysregulation of AQP4 and the DAC at the astrocytic endfoot likely contributes to the glymphatic dysfunction observed in Parkinson's disease, and that this impairment may exacerbate αSyn accumulation and pathology, establishing a positive feedback loop.

Data availability

Data are available on request.

Acknowledgements

Authors would like to thank Dr Phillip Muza and Miss Barbara Lechnicka for their critical appraisal of the manuscript.

Funding

This work was supported by research fellowship awards from both Parkinson's UK (F-1902) and Alzheimer's Research UK (ARUK-RF2019A-003) made to IFH.

Competing interests

The authors report no competing interests.

Supplementary material

Supplementary material is available at *Brain* online.

References

1. Li D, Liu C. Conformational strains of pathogenic amyloid proteins in neurodegenerative diseases. *Nature Reviews Neuroscience*. 2022/09/01 2022;23(9):523-534. doi:10.1038/s41583-022-00603-7

2. Lopes DM, Llewellyn SK, Harrison IF. Propagation of tau and α-synuclein in the brain: therapeutic potential of the glymphatic system. *Translational Neurodegeneration*. 2022/03/21 2022;11(1):19. doi:10.1186/s40035-022-00293-2

3. Goedert M, Falcon B, Clavaguera F, Tolnay M. Prion-like Mechanisms in the Pathogenesis of Tauopathies and Synucleinopathies. *Current Neurology and Neuroscience Reports*. 2014/09/14 2014;14(11):495. doi:10.1007/s11910-014-0495-z

4. Longhena F, Faustini G, Missale C, Pizzi M, Spano P, Bellucci A. The Contribution of α-Synuclein Spreading to Parkinson's Disease Synaptopathy. *Neural Plast*. 2017;2017:5012129. doi:10.1155/2017/5012129

5. Jessen NA, Munk AS, Lundgaard I, Nedergaard M. The Glymphatic System: A Beginner's Guide. *Neurochemical research*. Dec 2015;40(12):2583-99. doi:10.1007/s11064-015-1581-6

6. Kroesbergen E, Riesselmann LV, Gomolka RS, et al. Glymphatic clearance is enhanced during sleep. *bioRxiv*. 2024:2024.08.24.609514. doi:10.1101/2024.08.24.609514

7. Xie L, Kang H, Xu Q, et al. Sleep drives metabolite clearance from the adult brain. *Science*. Oct 18 2013;342(6156):373-7. doi:10.1126/science.1241224

8. Musiek ES, Holtzman DM. Mechanisms linking circadian clocks, sleep, and neurodegeneration. *Science (New York, NY)*. Nov 25 2016;354(6315):1004-1008. doi:10.1126/science.aah4968

9. Vanderheyden WM, Lim MM, Musiek ES, Gerstner JR. Alzheimer's Disease and Sleep–Wake Disturbances: Amyloid, Astrocytes, and Animal Models. *The Journal of Neuroscience*. 2018;38(12):2901. doi:10.1523/JNEUROSCI.1135-17.2017

10. Morawska MM, Moreira CG, Ginde VR, et al. Slow-wave sleep affects synucleinopathy and regulates proteostatic processes in mouse models of Parkinson's disease. *Science translational medicine*. 2021/12// 2021;13(623):eabe7099. doi:10.1126/scitranslmed.abe7099

11. Hablitz LM, Nedergaard M. The Glymphatic System: A Novel Component of Fundamental Neurobiology. *The Journal of Neuroscience*. 2021;41(37):7698. doi:10.1523/JNEUROSCI.0619-21.2021

12. Mestre H, Hablitz LM, Xavier AL, et al. Aquaporin-4-dependent glymphatic solute transport in the rodent brain. *eLife*. Dec 18 2018;7:40070. doi:10.7554/eLife.40070

13. Iliff JJ, Wang M, Liao Y, et al. A paravascular pathway facilitates CSF flow through the brain parenchyma and the clearance of interstitial solutes, including amyloid β. *Science translational medicine*. Aug 15 2012;4(147):147ra111. doi:10.1126/scitranslmed.3003748

14. Xu Z, Xiao N, Chen Y, et al. Deletion of aquaporin-4 in APP/PS1 mice exacerbates brain Aβ accumulation and memory deficits. *Molecular Neurodegeneration*. 2015/11/02 2015;10(1):58. doi:10.1186/s13024-015-0056-1

15. Harrison IF, Ismail O, Machhada A, et al. Impaired glymphatic function and clearance of tau in an Alzheimer's disease model. *Brain : a journal of neurology*. Aug 1 2020;143(8):2576-2593. doi:10.1093/brain/awaa179

16. Iliff JJ, Chen MJ, Plog BA, et al. Impairment of glymphatic pathway function promotes tau pathology after traumatic brain injury. *The Journal of neuroscience : the official journal of the Society for Neuroscience*. Dec 3 2014;34(49):16180-93. doi:10.1523/jneurosci.3020-14.2014

17. Ishida K, Yamada K, Nishiyama R, et al. Glymphatic system clears extracellular tau and protects from tau aggregation and neurodegeneration. *The Journal of experimental medicine*. Mar 7 2022;219:3. doi:10.1084/jem.20211275

18. Cui H, Wang W, Zheng X, et al. Decreased AQP4 Expression Aggravates α-Synuclein Pathology in Parkinson's Disease Mice, Possibly via Impaired Glymphatic Clearance. *Journal of molecular neuroscience : MN*. Dec 2021;71(12):2500-2513. doi:10.1007/s12031-021-01836-4

19. Zhang Y, Zhang C, He XZ, et al. Interaction Between the Glymphatic System and α-Synuclein in Parkinson's Disease. *Mol Neurobiol*. Apr 2023;60(4):2209-2222. doi:10.1007/s12035-023-03212-2

20. Simon M, Wang MX, Ismail O, et al. Loss of perivascular aquaporin-4 localization impairs glymphatic exchange and promotes amyloid β plaque formation in mice. *Alzheimer's research & therapy*. Apr 26 2022;14(1):59. doi:10.1186/s13195-022-00999-5

21. Hadjihambi A, Harrison IF, Costas-Rodríguez M, et al. Impaired brain glymphatic flow in experimental hepatic encephalopathy. *J Hepatol*. Jan 2019;70(1):40-49. doi:10.1016/j.jhep.2018.08.021

22. Pedersen TJ, Keil SA, Han W, Wang MX, Iliff JJ. The effect of aquaporin-4 mis-localization on Aβ deposition in mice. *Neurobiology of disease*. Jun 1 2023;181:106100. doi:10.1016/j.nbd.2023.106100

23. Kress BT, Iliff JJ, Xia M, et al. Impairment of paravascular clearance pathways in the aging brain. *Ann Neurol*. 2014;76(6):845-861. doi:10.1002/ana.24271

24. Zeppenfeld DM, Simon M, Haswell J, et al. Association of perivascular localization of aquaporin-4 with cognition and alzheimer disease in aging brains. *JAMA Neurology*. 2016;doi:10.1001/jamaneurol.2016.4370

25. Chen HL, Chen PC, Lu CH, et al. Associations among Cognitive Functions, Plasma DNA, and Diffusion Tensor Image along the Perivascular Space (DTI-ALPS) in Patients with Parkinson's Disease. *Oxid Med Cell Longev*. 2021;2021:4034509. doi:10.1155/2021/4034509

26. McKnight CD, Trujillo P, Lopez AM, et al. Diffusion along perivascular spaces reveals evidence supportive of glymphatic function impairment in Parkinson disease. *Parkinsonism Relat Disord*. Aug 2021;89:98-104. doi:10.1016/j.parkreldis.2021.06.004

27. Ma X, Li S, Li C, et al. Diffusion Tensor Imaging Along the Perivascular Space Index in Different Stages of Parkinson's Disease. *Front Aging Neurosci*. 2021;13:773951. doi:10.3389/fnagi.2021.773951

28. Cai X, Chen Z, He C, et al. Diffusion along perivascular spaces provides evidence interlinking compromised glymphatic function with aging in Parkinson's disease. *CNS Neurosci Ther*. Jan 2023;29(1):111-121. doi:10.1111/cns.13984

29. Qin Y, He R, Chen J, et al. Neuroimaging uncovers distinct relationships of glymphatic dysfunction and motor symptoms in Parkinson's disease. *J Neurol*. May 2023;270(5):2649-2658. doi:10.1007/s00415-023-11594-5

30. Wood KH, Nenert R, Miften AM, et al. Diffusion Tensor Imaging-Along the Perivascular-Space Index Is Associated with Disease Progression in Parkinson's Disease. *Mov Disord*. Jul 11 2024;doi:10.1002/mds.29908

31. Shi C, Guo G, Wang W, et al. Impaired glymphatic clearance in multiple system atrophy: A diffusion spectrum imaging study. *Parkinsonism Relat Disord*. Jun 2024;123:106950. doi:10.1016/j.parkreldis.2024.106950

32. Polinski NK, Volpicelli-Daley LA, Sortwell CE, et al. Best Practices for Generating and Using Alpha-Synuclein Pre-Formed Fibrils to Model Parkinson's Disease in Rodents. *J Parkinsons Dis*. 2018;8(2):303-322. doi:10.3233/jpd-171248

33. Giasson BI, Duda JE, Quinn SM, Zhang B, Trojanowski JQ, Lee VM. Neuronal alpha-synucleinopathy with severe movement disorder in mice expressing A53T human alpha-synuclein. *Neuron*. May 16 2002;34(4):521-33. doi:10.1016/s0896-6273(02)00682-7

34. Lopes DM, Wells JA, Ma D, et al. Glymphatic inhibition exacerbates tau propagation in an Alzheimer's disease model. *Alzheimers Res Ther*. Apr 5 2024;16(1):71. doi:10.1186/s13195-024-01439-2

35. Yushkevich PA, Piven J, Hazlett HC, et al. User-guided 3D active contour segmentation of anatomical structures: Significantly improved efficiency and reliability. *NeuroImage*. 2006/07/01/ 2006;31(3):1116-1128. doi:https://doi.org/10.1016/j.neuroimage.2006.01.015

36. Luk KC, Kehm VM, Zhang B, O'Brien P, Trojanowski JQ, Lee VM. Intracerebral inoculation of pathological α-synuclein initiates a rapidly progressive neurodegenerative α-synucleinopathy in mice. *The Journal of experimental medicine*. May 7 2012;209(5):975-86. doi:10.1084/jem.20112457

37. Chau KY, Ching HL, Schapira AH, Cooper JM. Relationship between alpha synuclein phosphorylation, proteasomal inhibition and cell death: relevance to Parkinson's disease pathogenesis. *J Neurochem*. Aug 2009;110(3):1005-13. doi:10.1111/j.1471-4159.2009.06191.x

38. Ringstad G. Glymphatic imaging: a critical look at the DTI-ALPS index. *Neuroradiology*. 2024/02/01 2024;66(2):157-160. doi:10.1007/s00234-023-03270-2

39. Zeppenfeld DM, Simon M, Haswell JD, et al. Association of Perivascular Localization of Aquaporin-4 With Cognition and Alzheimer Disease in Aging Brains. *JAMA Neurology*. 2017;74(1):91-99. doi:10.1001/jamaneurol.2016.4370

40. Hoshi A, Tsunoda A, Tada M, Nishizawa M, Ugawa Y, Kakita A. Expression of Aquaporin 1 and Aquaporin 4 in the Temporal Neocortex of Patients with Parkinson's Disease. *Brain Pathol*. Mar 2017;27(2):160-168. doi:10.1111/bpa.12369

41. Zamani A, Walker AK, Rollo B, et al. Impaired glymphatic function in the early stages of disease in a TDP-43 mouse model of amyotrophic lateral sclerosis. *Transl Neurodegener*. Mar 15 2022;11(1):17. doi:10.1186/s40035-022-00291-4

42. Liu H, Chen L, Zhang C, et al. Glymphatic influx and clearance are perturbed in Huntington's disease. *JCI insight*. Sep 3 2024;doi:10.1172/jci.insight.172286

43. Robinson JL, Xie SX, Baer DR, et al. Pathological combinations in neurodegenerative disease are heterogeneous and disease-associated. *Brain : a journal of neurology*. 2023;146(6):2557-2569. doi:10.1093/brain/awad059

44. Boyle PA, Wang T, Yu L, et al. To what degree is late life cognitive decline driven by age-related neuropathologies? *Brain : a journal of neurology*. Aug 17 2021;144(7):2166-2175. doi:10.1093/brain/awab092

45. Kapasi A, DeCarli C, Schneider JA. Impact of multiple pathologies on the threshold for clinically overt dementia. *Acta neuropathologica*. Aug 2017;134(2):171-186. doi:10.1007/s00401-017-1717-7

46. Spina S, La Joie R, Petersen C, et al. Comorbid neuropathological diagnoses in early versus late-onset Alzheimer's disease. *Brain : a journal of neurology*. 2021;144(7):2186-2198. doi:10.1093/brain/awab099

47. Zou W, Pu T, Feng W, et al. Blocking meningeal lymphatic drainage aggravates Parkinson's disease-like pathology in mice overexpressing mutated α-synuclein. *Translational Neurodegeneration*. 2019/03/01 2019;8(1):7. doi:10.1186/s40035-019-0147-y

48. Hablitz LM, Vinitsky HS, Sun Q, et al. Increased glymphatic influx is correlated with high EEG delta power and low heart rate in mice under anesthesia. *Sci Adv*. Feb 2019;5(2):eaav5447. doi:10.1126/sciadv.aav5447

49. Bèchet NB, Shanbhag NC, Lundgaard I. Glymphatic pathways in the gyrencephalic brain. *J Cereb Blood Flow Metab*. Sep 2021;41(9):2264-2279. doi:10.1177/0271678x21996175

50. Braak H, Tredici KD, Rüb U, de Vos RAI, Jansen Steur ENH, Braak E. Staging of brain pathology related to sporadic Parkinson's disease. *Neurobiology of Aging*. 2003/03/01/ 2003;24(2):197-211. doi:https://doi.org/10.1016/S0197-4580(02)00065-9

51. Si X, Dai S, Fang Y, et al. Matrix metalloproteinase-9 inhibition prevents aquaporin-4 depolarization-mediated glymphatic dysfunction in Parkinson's disease. *Journal of Advanced Research*. 2024/02/01/ 2024;56:125-136. doi:https://doi.org/10.1016/j.jare.2023.03.004

52. Russo I, Bubacco L, Greggio E. LRRK2 and neuroinflammation: partners in crime in Parkinson's disease? *J Neuroinflammation*. Mar 21 2014;11:52. doi:10.1186/1742-2094-11-52

53. Huang H, Lin L, Wu T, et al. Phosphorylation of AQP4 by LRRK2 R1441G impairs glymphatic clearance of IFNγ and aggravates dopaminergic neurodegeneration. *NPJ Parkinsons Dis*. Jan 31 2024;10(1):31. doi:10.1038/s41531-024-00643-z

54. Peng W, Yuan Y, Lei J, et al. Long-Term High-Fat Diet Impairs AQP4-Mediated Glymphatic Clearance of Amyloid Beta. *Molecular Neurobiology*. 2024/07/03 2024;doi:10.1007/s12035-024-04320-3

55. Chen Z, Lai JHC, Xu J, Zhang H, Huang J, Chan KWY. The effect of aquaporin-4 inhibition on cerebrospinal fluid-tissue water exchange in mouse brain detected by magnetization transfer indirect spin labeling MRI. *NMR Biomed*. Jul 2024;37(7):e5093. doi:10.1002/nbm.5093

56. Li X, Xie Z, Zhou Q, et al. TGN-020 Alleviate Inflammation and Apoptosis After Cerebral Ischemia-Reperfusion Injury in Mice Through Glymphatic and ERK1/2 Signaling Pathway. *Mol Neurobiol*. Feb 2024;61(2):1175-1186. doi:10.1007/s12035-023-03636-w

57. Huang W, Zhang Y, Zhou Y, et al. Glymphatic Dysfunction in Migraine Mice Model. *Neuroscience*. Sep 15 2023;528:64-74. doi:10.1016/j.neuroscience.2023.07.027

58. Lv C, Han S, Sha Z, et al. Cerebral glucagon-like peptide-1 receptor activation alleviates traumatic brain injury by glymphatic system regulation in mice. *CNS Neurosci Ther*. Dec 2023;29(12):3876-3888. doi:10.1111/cns.14308

59. Takano K, Yamada M. Contrast-enhanced magnetic resonance imaging evidence for the role of astrocytic aquaporin-4 water channels in glymphatic influx and interstitial solute

transport. *Magnetic Resonance Imaging*. 2020/09/01/ 2020;71:11-16. doi:https://doi.org/10.1016/j.mri.2020.05.001

60. Huber VJ, Tsujita M, Nakada T. Identification of Aquaporin 4 inhibitors using in vitro and in silico methods. *Bioorganic & Medicinal Chemistry*. 2009/01/01/ 2009;17(1):411-417. doi:10.1016/j.bmc.2007.12.040

61. Verkman AS, Smith AJ, Phuan PW, Tradtrantip L, Anderson MO. The aquaporin-4 water channel as a potential drug target in neurological disorders. *Expert Opin Ther Targets*. Dec 2017;21(12):1161-1170. doi:10.1080/14728222.2017.1398236

62. Salman MM, Kitchen P, Yool AJ, Bill RM. Recent breakthroughs and future directions in drugging aquaporins. *Trends in Pharmacological Sciences*. 2022;43(1):30-42. doi:10.1016/j.tips.2021.10.009

63. Polinski NK. A Summary of Phenotypes Observed in the In Vivo Rodent Alpha-Synuclein Preformed Fibril Model. *J Parkinsons Dis*. 2021;11(4):1555-1567. doi:10.3233/jpd-212847

64. Earls RH, Menees KB, Chung J, et al. NK cells clear α-synuclein and the depletion of NK cells exacerbates synuclein pathology in a mouse model of α-synucleinopathy. *Proc Natl Acad Sci U S A*. Jan 21 2020;117(3):1762-1771. doi:10.1073/pnas.1909110117

Figure legends

Figure 1 αSyn PFFs exhibit amyloid characteristics and induce propagation *in vitro* and *in vivo.* Aggregates are present in generated PFFs, as is evident by their sedimentation following centrifugation. (**A**) Coomassie stained electrophoresis gel showing that the majority of the protein (14 kDa, αSyn) is in the supernatant of the monomer starting material, but in the pellet of generated PFFs following centrifugation. Results from this assay are shown graphically in (**B**). Generated PFFs fluoresce with ThT (**C**) indicating the presence of amyloid structures. Both sonicated and unsonicated PFFs are also immunopositive for a commonly used conformation-specific αSyn antibody (MJFR-14-6-4-2) (**D**, **E**), indicating the presence of aggregated αSyn protein in generated PFFs. Sonicated and unsonicated PFF also induce a stepwise left-ward shift in the sigmoidal

intensity profile of ThT monitored αSyn aggregation *in vitro* (**F**), resulting in reduced $Time_{50}$ values in PFF seeded samples compared to aggregate formation of monomers alone (**F, inset**). PFFs were also shown to induce propagation of αSyn *in vitro* in a cell culture system. Incubation of SH-SY5Y cells over expressing HA-tagged αSyn caused the increased accumulation of insoluble pS129 αSyn, aggregation of endogenously expressed (HA-tagged) αSyn and the occurrence of higher molecular weight (HMW) αSyn species (**G**, arrows). (**H**) Immunofluorescence images of αSyn pathology (aggregate conformation-specific) in the striatum (both ipsilateral and contralateral) of monomer and PFF injected M83 mice, illustrating both intracellular αSyn accumulations (arrowheads) and αSyn neurite pathology (arrows) in PFF injected but not monomer injected animals. Results from statistical tests (C and F inset, 1-way ANOVA; B, 2-way ANOVA) indicated with asterisks: **=p<0.01, ****=p<0.0001.

Figure 2 αSyn PFF seeding causes dystrophin associated complex dysregulation *in vivo*. (**A**) Striatal mRNA expression levels of AQP4 and DAC elements in experimental groups injected with either αSyn monomers or PFFs and left to age for 2, 4 or 6 weeks. Expression data is normalised to wildtype baseline expression levels (dotted line). (**B**) Diagrammatic illustration of the DAC at the astrocytic endfoot membrane, with elements colour-coded to reflect data in (A). (**C**) Individual animal datapoints (N=8) shown in heatmap. (**D**) Correlation analysis of mRNA expression profiles with animal-by-animal αSyn load data, illustrating significant negative correlations with AQP4 and SNTA1, and correlations approaching significance in the other three DAC proteins. Results from statistical tests (A, 2-way ANOVA; D, simple linear regression fitting) indicated with asterisks: *=p<0.05, ****=p<0.0001. Asterisks in (A) indicate significance from M83 baseline (BL), asterisks with bars indicate timepoint comparisons. N=8 per group/timepoint.

Figure 3 αSyn arrival coincides with glymphatic upregulation in the midbrain of PFF seeded mice. (**A**) Fluorescence intensity in the midbrain (solid outline) in brain sections (dashed outline) following cisterna magna infusion of Texas Red™-conjugated dextran (3 kDa). Intensity is quantified and graphed in (**B**) illustrating increased midbrain uptake at 4 and 6 weeks post-PFF injection. The ipsilateral midbrain area is illustrated with empty bars, the contralateral midbrain area is illustrated with hashed bars. (**C**) Quantification of αSyn at these same timepoints showed a

surge of αSyn deposition at week 4, which resolves by week 6 after PFF injection. (**D**) Representative blots for data presented in (C). Results from statistical tests (B, 2-way ANOVA; C, 1-way ANOVA) indicated with asterisks: *=p<0.05, **=p<0.01, ***=p<0.001. N=3-8 per group/timepoint.

Figure 4 Acute TGN-020 treatment reduces brain to CSF αSyn clearance. (**A**) Diagrammatic representation and (**B**) time course of acute experiments, illustrating intrastriatal injection of aCSF or PFFs and pre-treatment with vehicle or TGN-020 (50 mg/kg). TGN-020 results in elevated levels of PFF brain retention (**C**) and a corresponding reduction in clearance to CSF (**D**). Results from statistical tests (1-way ANOVAs) indicated with asterisks: *=p<0.05, **=p<0.01, ***=p<0.001. N=5-6 per group.

Figure 5 Chronic TGN-020 treatment induces behavioural deficits in the PFF-M83 model of αSyn propagation. (**A**) Diagrammatic representation and (**B**) time course of chronic experiments, illustrating location of intracerebral injection (striatum and overlying cortex) of either monomers or PFFs, followed by chronic treatment with TGN-020 (50 mg/kg, 3 times/week) for 6 weeks, with behavioural test and structural MRI acquisition timepoints noted. TGN-020 treatment resulted in reduced distance travelled in an open field arena after 6 weeks of treatment compared to baseline assessment (**C**), and increased immobility (**D**). Results from statistical tests (2-way ANOVAs) indicated with asterisks: **=p<0.01, ***=p<0.001. N=8-9 per group.

Figure 6 Chronic TGN-020 treatment exacerbates pathology in the PFF-M83 model of αSyn propagation. Volumes of the (**A**) striatum and (**B**) midbrain in chronically treated mice, indicating exacerbation of αSyn PFF induced atrophy following chronic treatment with TGN-020 for 6 weeks. (**C**) Representative immunofluorescence images of αSyn pathology (aggregate conformation-specific) in the striatum of treated mice, quantified and presented in (**D**), illustrating increased αSyn pathology with TGN-020 treatment. A corresponding decrease of CSF αSyn was observed in experimental animals. Results from statistical tests (A, B and C, 2-way ANOVAs; D, 1-way ANOVA) indicated with asterisks: *=p<0.05, **=p<0.01, ***=p<0.001, ****=p<0.0001.

Asterisks without bars indicate individual hemispheric differences compared to the M83^{Mons} Vehicle group. *N*=5-9 per group.

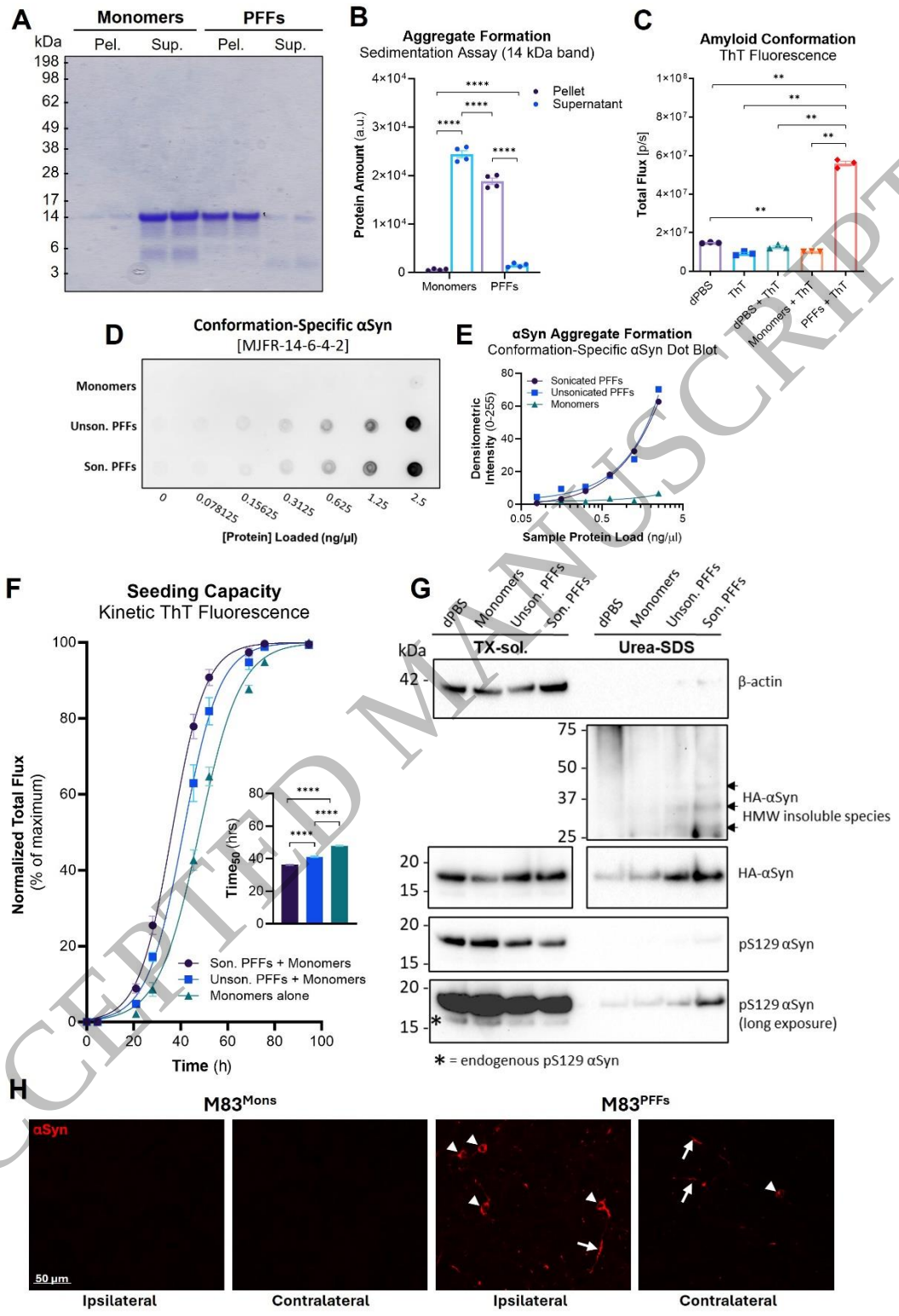

Figure 1
187x272 mm (x DPI)

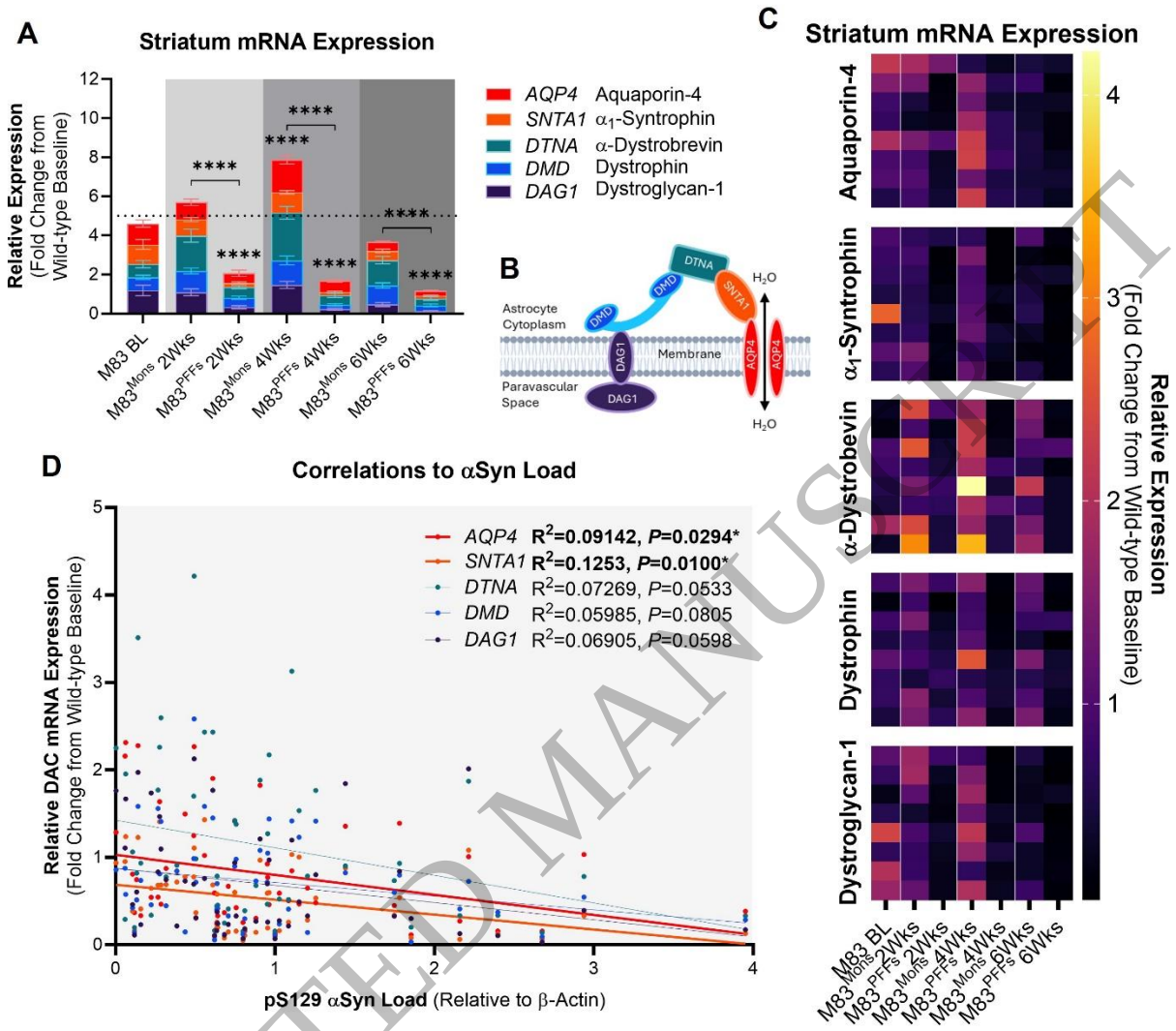

Figure 2
232x203 mm (x DPI)

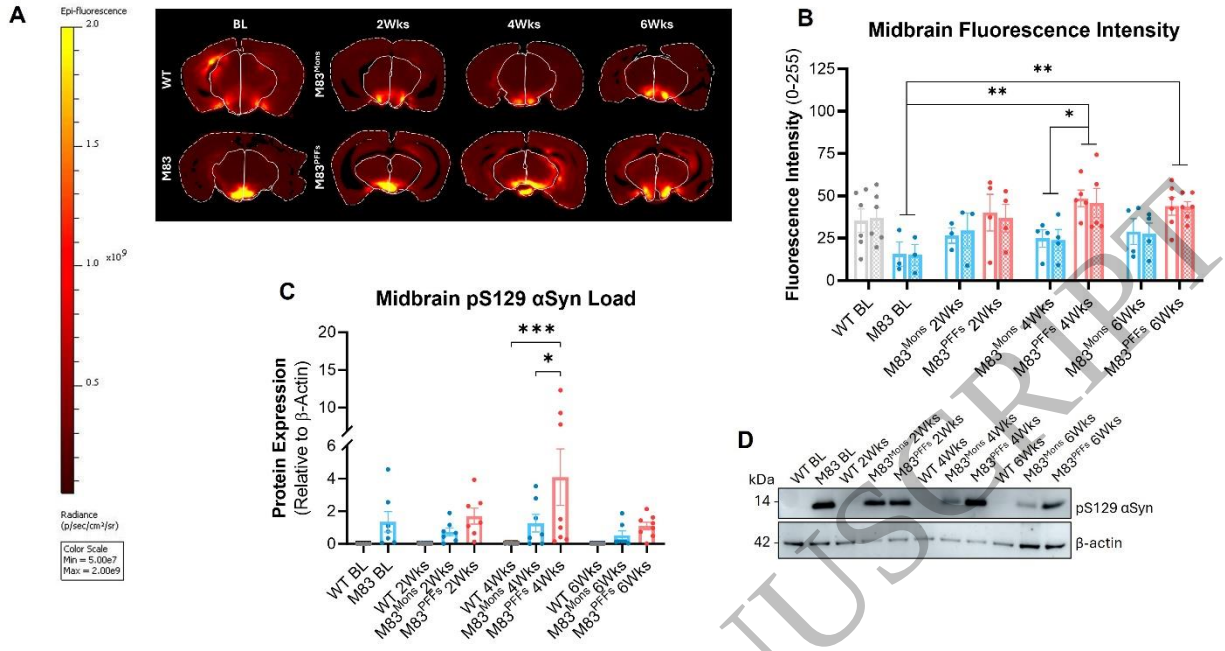

Figure 3
300x171 mm (x DPI)

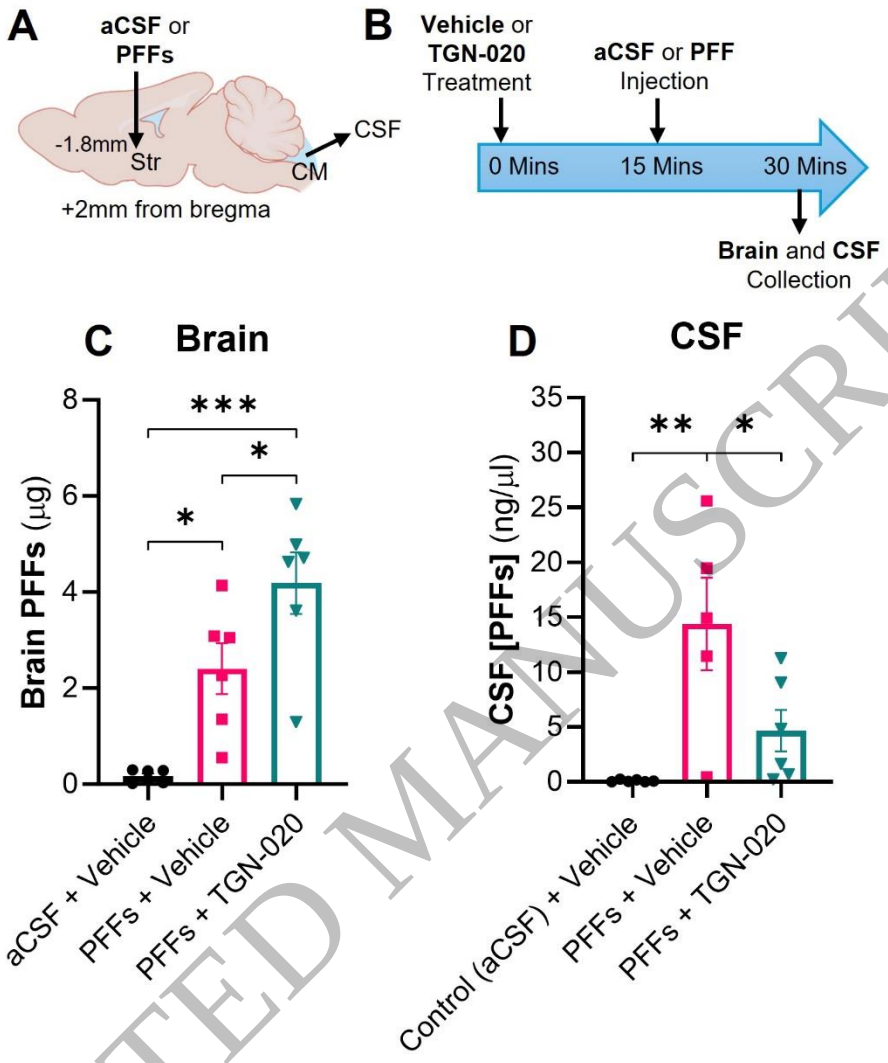

Figure 4
123x145 mm (x DPI)

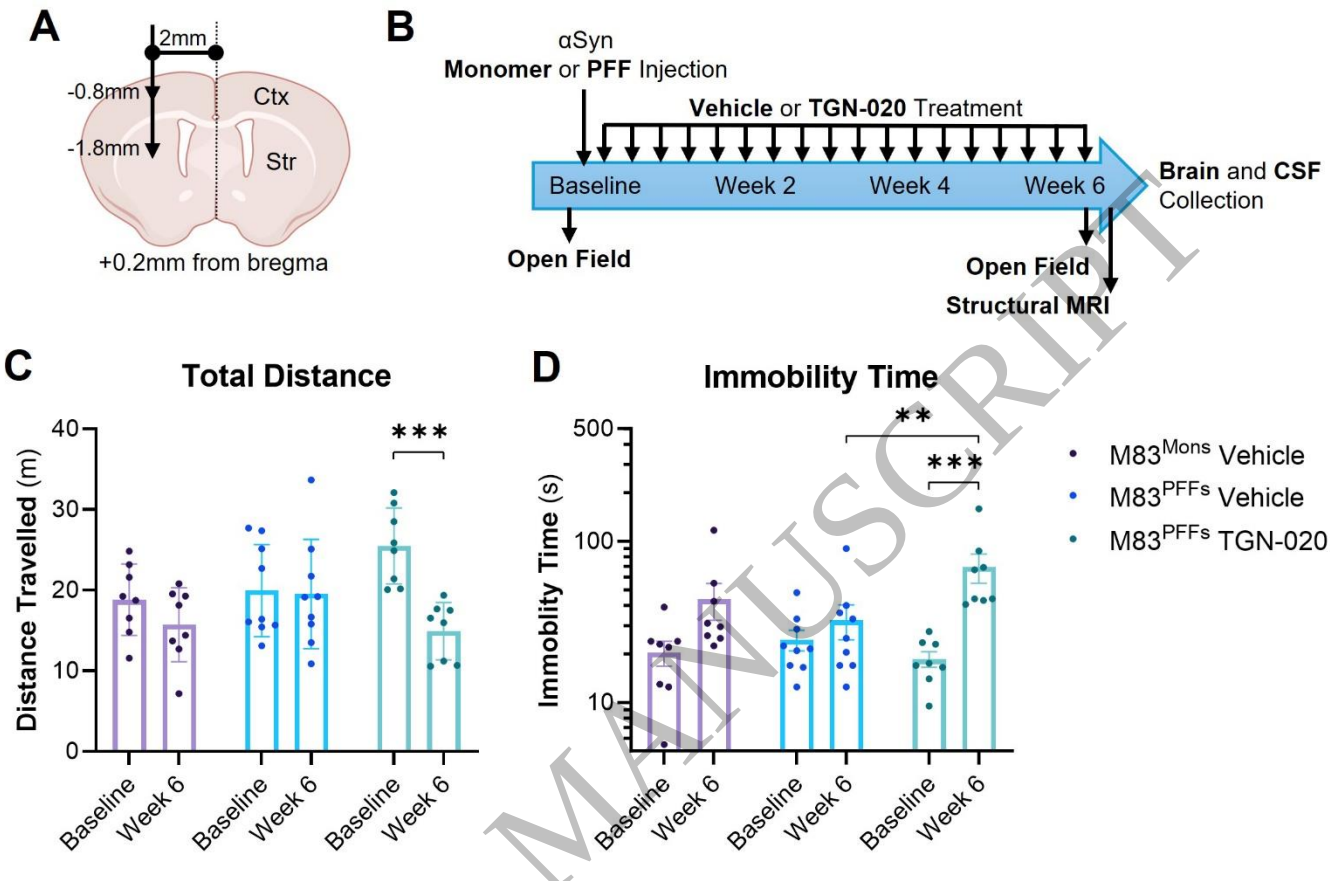

Figure 5
182x118 mm (x DPI)

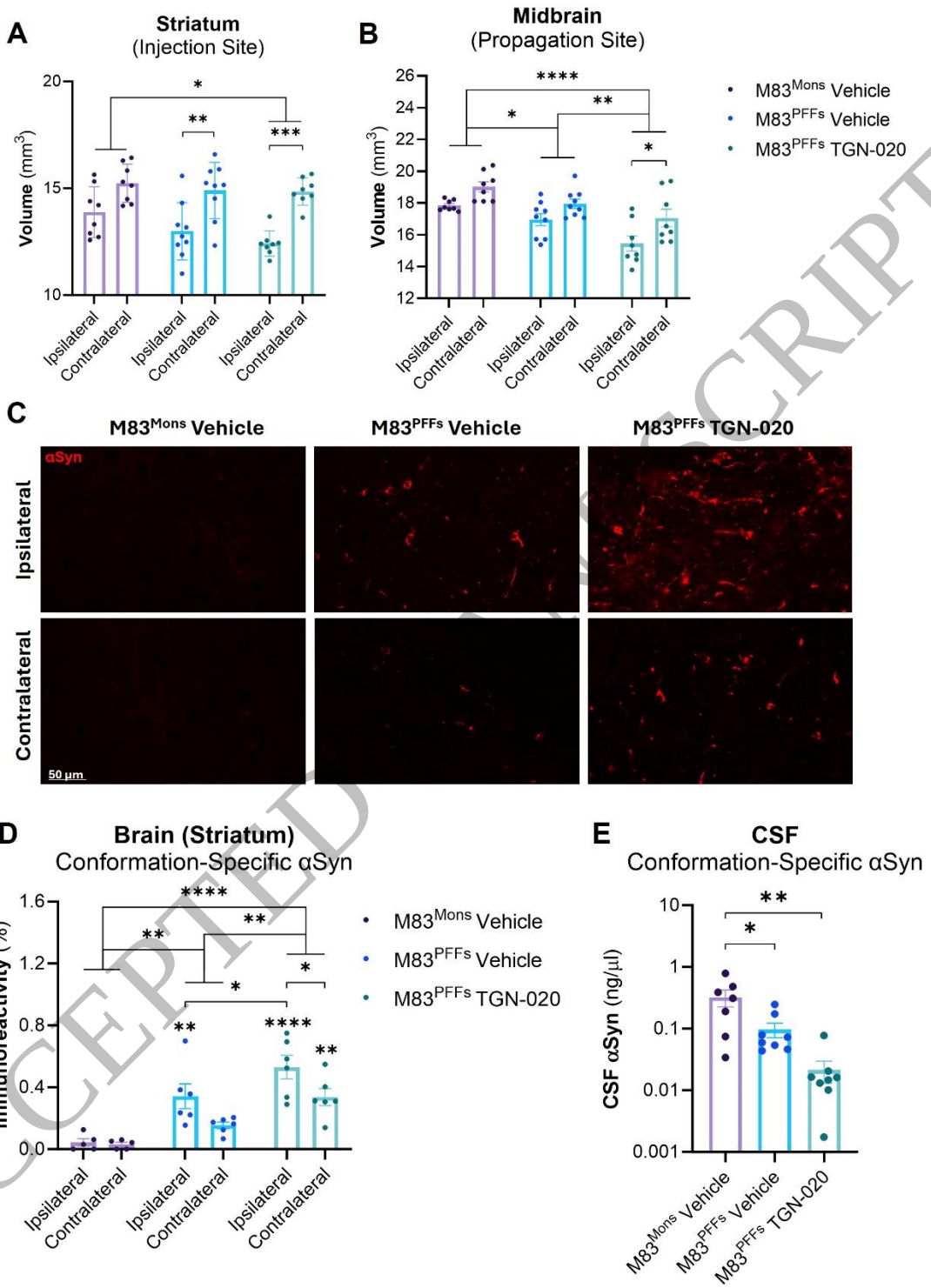

Figure 6
188x255 mm (x DPI)

TYSABRI™ (natalizumab)
SUBCUTANEOUS USE | 300mg

Prescribing Information

Efficacy made Convenient

TYSABRI SC injection with the potential to administer **AT HOME** for eligible patients*

Efficacy and safety profile comparable between TYSABRI IV and SC†[1,2]

†Comparable PK, PD, efficacy, and safety profile of SC to IV except for injection site pain.[1,2]

CLICK HERE TO DISCOVER MORE ABOUT TYSABRI SC AND THE DIFFERENCE IT MAY MAKE TO YOUR ELIGIBLE PATIENTS

Supported by

BIOGEN'S Stratify JCV™ SERVICE

A Biogen developed and funded JCV antibody index PML risk stratification service, validated and available exclusively for patients on or considering TYSABRI.

*As of April 2024, TYSABRI SC can be administered outside a clinical setting (e.g. at home) by a HCP for patients who have tolerated at least 6 doses of TYSABRI well in a clinical setting. Please refer to section 4.2 of the SmPC.[1]

TYSABRI is indicated as single DMT in adults with highly active RRMS for the following patient groups:[1,2]

- **Patients with highly active disease despite a full and adequate course of treatment with at least one DMT**
- **Patients with rapidly evolving severe RRMS defined by 2 or more disabling relapses in one year, and with 1 or more Gd+ lesions on brain MRI or a significant increase in T2 lesion load as compared to a previous recent MRI**

Very common AEs include nasopharyngitis and urinary tract infection. Please refer to the SmPC for further safety information, including the risk of the uncommon but serious AE, PML.[1,2]

Abbreviations: AE: Adverse Event; **DMT:** Disease-Modifying Therapy; **Gd+:** Gadolinium-Enhancing; **HCP:** Healthcare Professional; **IV:** Intravenous; **JCV:** John Cunningham Virus; **MRI:** Magnetic Resonance Imaging; **PD:** Pharmacodynamic; **PK:** Pharmacokinetic; **PML:** Progressive Multifocal Leukoencephalopathy; **RRMS:** Relapsing-Remitting Multiple Sclerosis; **SC:** Subcutaneous.

References: 1. TYSABRI SC (natalizumab) Summary of Product Characteristics. **2.** TYSABRI IV (natalizumab) Summary of Product Characteristics.

Adverse events should be reported. For Ireland, reporting forms and information can be found at www.hpra.ie. For the UK, reporting forms and information can be found at https://yellowcard.mhra.gov.uk/ or via the Yellow Card app available from the Apple App Store or Google Play Store. Adverse events should also be reported to Biogen Idec on MedInfoUKI@biogen.com 1800 812 719 in Ireland and 0800 008 7401 in the UK.

Biogen-261128. DOP: April 2025

Biogen